Impact of vegetation on flow routing and sedimentation patterns: Three-dimensional modeling for a tidal marsh

S. Temmerman,[1,2] T. J. Bouma,[1] G. Govers,[3] Z. B. Wang,[4] M. B. De Vries,[4] and P. M. J. Herman[1]

[1] A three-dimensional hydrodynamic and sediment transport model was used to study the relative impact of (1) vegetation, (2) micro-topography, and (3) water level fluctuations on the spatial flow and sedimentation patterns in a tidal marsh landscape during single inundation events. The model incorporates three-dimensional (3-D) effects of vegetation on the flow (drag and turbulence). After extensive calibration and validation against field data, the model showed that the 3-D vegetation structure is determinant for the flow and sedimentation patterns. As long as the water level is below the top of the vegetation, differences in flow resistance between vegetated and unvegetated areas result in faster flow routing over unvegetated areas, so that vegetated areas are flooded from unvegetated areas, with flow directions more or less perpendicular to the vegetation edge. At the vegetation edge, flow velocities are reduced and sediments are rapidly trapped. In contrast, in between vegetated areas, flow velocities are enhanced, resulting in reduced sedimentation or erosion. As the water level overtops the vegetation, the flow paths described above change to more large-scale sheet flow crossing both vegetated and unvegetated areas. As a result, sedimentation patterns are then spatially more homogeneous. Our results suggest that the presence of a vegetation cover is the key factor controlling the long-term geomorphic development of tidal marsh landforms, leading to the formation of (1) unvegetated tidal channels and (2) vegetated platforms with a levee-basin topography in between these channels.

1. Introduction

[2] Flow paths of water and its constituents (sediments, nutrients, contaminants) strongly determine the functioning of wetlands, such as floodplains and tidal marshes. These wetland types are periodically flooded, either fluvially or tidally, during which suspended sediments, nutrients and contaminants are spatially distributed by the flooding water and partly deposited within the system. The resulting spatial depositional patterns, which occur on the timescale of single flood events, are the key to the understanding of the long-term (10–100 years) geomorphic and ecological dynamics of tidal marshes and floodplains. Sediment deposition determines their response to global change; for example, it determines the ability of tidal marshes to keep up with expected accelerations in sea level rise [e.g., *Temmerman et al.*, 2004b]. Spatial sedimentation patterns lead to geomorphic heterogeneity, which in its turn has a strong control on habitat diversity and biodiversity [*Nichols et al.*, 1998].

[3] In general, flow paths of water and constituents over vegetated wetlands are determined by (1) water discharge or water level fluctuations, (2) topography and (3) vegetation cover. However, the relative importance of each of these factors and how they interact and contribute to the overall spatial flow and sedimentation pattern is poorly understood. This is related to a lack of experimental data. Field monitoring of high-resolution two- or three-dimensional flow patterns is extremely difficult owing to practical problems, such as the difficulty to predict flood events, restricted field accessibility during these flood events, and the large amount of field equipment and manpower that is needed. Furthermore, it is nearly impossible to conduct field experiments on a landscape scale (i.e., length scales of 10^2–10^3 m), in which water levels, topography and vegetation are manipulated in order to quantify their relative influence on the spatial flow and sedimentation pattern.

[4] In this respect, modeling offers an opportunity to conduct numerical experiments. Hydrodynamic models, based on a solution of the shallow-water equations, are increasingly being used to study flow and constituent

[1]Centre for Estuarine and Marine Ecology, Netherlands Institute of Ecology (NIOO-KNAW), Yerseke, Netherlands.
[2]Now at Department of Biology, University of Antwerpen, Antwerpen, Belgium.
[3]Physical and Regional Geography Research Group, Catholic University of Leuven, Leuven, Belgium.
[4]WL|Delft Hydraulics, Delft, Netherlands.

transport processes in a variety of environments (rivers, estuaries, coastal seas), in two or three dimensions and with a spatial and temporal resolution that can hardly be reached in field studies [*Lane*, 1998]. Such hydrodynamic models have been applied also to vegetated wetlands, in particular to floodplains [e.g., *Bates et al.*, 1996; *Beffa and Connell*, 2001; *Horritt*, 2000; *Nicholas and Mitchell*, 2003]. In these floodplain model studies, the influence of vegetation on flow hydrodynamics is traditionally simulated in an indirect way, using a two-dimensional depth-averaged model and using a high roughness coefficient for vegetated surfaces. Such an approach, however, does not account for the influence of vegetation over the whole water depth but only near the bed and therefore does not allow the study of the three-dimensional influence of the vegetation canopy on the flow (e.g., different flow patterns within and above the vegetation canopy).

[5] Recent laboratory flume studies have enlarged our insights on drag and turbulence caused by vegetation and its different effects on vertical flow and turbulence profiles within and above the vegetation canopy [e.g., *Nepf*, 1999; *Nepf and Vivoni*, 2000]. These mechanisms have been incorporated in hydrodynamic models, including additional formulations for drag and turbulence generated by cylindrical plant structures at different depths within the water column [e.g., *Fischer-Antze et al.*, 2001; *Lopez and Garcia*, 2001; *Neary*, 2003]. Until now, these plant-flow interaction models were applied and tested on the small scale of a laboratory flume (1–10 m). On the large scale of a landscape (10^2–10^3 m), model studies of the three-dimensional influence of vegetation on flow and sedimentation patterns are lacking, mainly because field data for model calibration and validation are not available.

[6] In this study we apply a three-dimensional plant-flow interaction model to a tidal marsh landscape. The topography of tidal marshes typically consists of a vegetated marsh platform, dissected by dense networks of unvegetated tidal channels or creeks and with a levee-basin micro-topography in between these creeks. Flow paths over tidal marshes are relatively poorly documented (see *Allen* [2000] for an overview). Flow hydrodynamics and sediment transport have been measured extensively in tidal channels, because these channels were traditionally considered as conduits for water and suspended sediment from the open sea to and from tidal marshes [e.g., *Bayliss-Smith et al.*, 1979; *Bouma et al.*, 2005a; *French and Stoddart*, 1992; *Reed et al.*, 1985]. However, not all water exchange takes place via tidal channels, but considerable amounts of water are transported as sheet flow directly from the seaward marsh edge over the marsh platform [*French and Stoddart*, 1992; *Temmerman et al.*, 2005]. The few studies that measured flow patterns above the vegetated marsh platform suggest that flow directions may vary in a complex way from perpendicular to parallel to tidal channels [*Christiansen et al.*, 2000; *Davidson-Arnott et al.*, 2002; *Leonard*, 1997; *Wang et al.*, 1993]. The vertical flow profile above the marsh platform is strongly affected by the marsh vegetation [e.g., *Leonard and Luther*, 1995; *Shi et al.*, 1995]. Spatial sedimentation patterns are traditionally related to the marsh topography: Sedimentation rates were shown to decrease with increasing marsh surface elevation (i.e., decreasing inundation frequency), increasing distance from the seaward marsh edge

and increasing distance from creeks (i.e., selective sediment trapping along flow paths) [e.g., *French and Spencer*, 1993; *Leonard*, 1997; *Temmerman et al.*, 2003].

[7] Thus existing field data on flow and sedimentation patterns in tidal marshes are very fragmentary and limited to rather local flow hydrodynamics, either measured in unvegetated tidal channels or above the vegetated marsh platform. Large-scale (whole system) two- or three-dimensional patterns, including interactions between tidal channel and marsh platform flow, are so far not documented. Up to now, studies modeling the spatial flow patterns in tidal marshes are rather limited, using a one- or two-dimensional approach, neglecting the micro-topography of a marsh platform by assuming a flat surface and/or neglecting the three-dimensional influence of vegetation on flow hydrodynamics [e.g., *Allen*, 1994; *Fagherazzi and Sun*, 2004; *Lawrence et al.*, 2004; *Marani et al.*, 2003; *Mudd et al.*, 2004; *Rinaldo et al.*, 1999; *Woolnough et al.*, 1995]. As a consequence, we have poor knowledge on the relative impact of the vegetation structure and micro-topography on the spatial flow patterns over a natural tidal marsh and to what extent these spatial flow patterns are changing with time, for example, as the water level changes from within to above the vegetation canopy during an inundation cycle.

[8] The aim of this study is to quantify the relative impact of water level fluctuations, micro-topography and vegetation on the spatial flow and sedimentation patterns in a tidal marsh, for a single tidal cycle. A three-dimensional hydrodynamic and sediment transport model (Delft3D), incorporating small-scale plant-flow interactions, is applied on the large scale of a natural tidal marsh (Paulina marsh, SW Netherlands). First, the model is extensively calibrated and validated using a field data set on hydrodynamics and sediment transport. Second, once validated, the model is used to quantify the relative influence of different factors on the spatial flow and sedimentation pattern, such as tidal inundation height, micro-topography and vegetation structure. Our simulations demonstrate that the presence of a vegetation cover is the most crucial factor that controls the spatial flow and sedimentation patterns on a tidal marsh, for a single tidal cycle. Implications for the long-term formation of tidal marsh landforms are discussed.

2. Study Area

[9] The Delft3D model was applied to a tidal creek catchment (5.6 ha) within the Paulina salt marsh in the Scheldt estuary, SW Netherlands (Figure 1). The local tidal regime is semi-diurnal, with a mean tidal range of 3.9 m. Different stages in the geomorphological development and vegetational succession of salt marshes are present within the studied creek catchment: (1) an old, high marsh (already present on topographic maps of 1856) and (2) a young, low marsh (formed around 1980) (Figures 1b and 1c). The high marsh is characterized by a relatively flat marsh platform dissected by a well-developed network of tidal creeks that widen (0.3–7 m), deepen (0.3–1.5 m) and converge in the seaward direction. The maximum distance between creeks is about 40 m. The high marsh platform exhibits a micro-topography of levees and basins. The levees are just next to the creeks and are 0.2–0.3 m higher than the basins, which are 10–30 m from the creeks (Figures 1b and 1c). During an
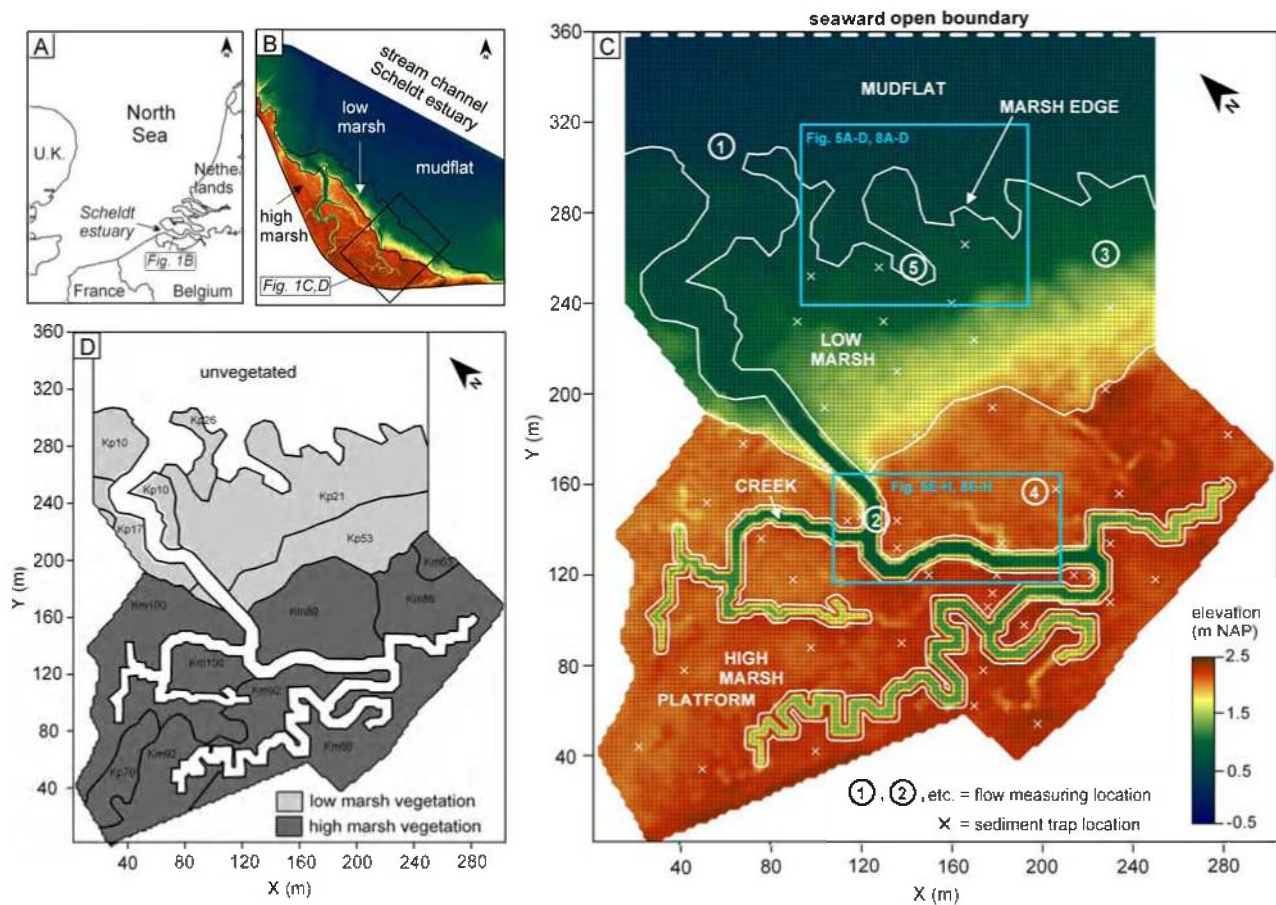
Figure 1. (a) Location of the study area in NW Europe. (b) Location of the studied tidal creek catchment within the Paulina marsh (SW Netherlands). (c) The computational grid of the tidal creek catchment: the grid is represented in thin black lines, the marsh surface elevation in each grid cell is indicated in color scale, the seaward open boundary in broken white line, geomorphic zones with white lines and white labels (e.g., CREEK), flow measuring locations in white encircled numbers, sediment trap locations as white crosses. Blue boxes indicate areas plotted in Figure 5 and 8. (d) Vegetation map [after *Koppejan*, 2000]: light gray zones represent low marsh vegetation types (dominated by *Spartina anglica*), and dark gray zones represent high marsh vegetation types (dominated by *Puccinellia maritima*, *Limonium vulgare* and *Halimione portulacoides*). The labels of vegetation types (Kp 21, etc.) are explained in Table 2.

average spring tide, the high water level is about 0.4 m above the basins. The high marsh platform is vegetated by NW European salt marsh species, such as *Puccinellia maritima*, *Limonium vulgare* and *Halimione portulacoides*. The low marsh has a contrasting morphology. It gradually slopes down to the seaward marsh edge and has only few tidal creeks and no levee-basin topography (Figures 1b and 1c). During an average spring tide, the high water level ranges from 0.4 to 1.6 m above the low marsh surface. This low marsh is vegetated by *Spartina anglica*. The bed material of the marsh and tidal creeks consists of mud. Beyond the seaward marsh edge is an unvegetated tidal mudflat.

3. Methods

3.1. Brief Description of the Model

[10] We used the Delft3D software package, which is a computational fluid dynamics model that allows simulation of flow hydrodynamics and transport phenomena [e.g.,

Hibma et al., 2003; *Lesser et al.*, 2004]. Below we give a brief description of the Delft3D modules that we used for this study: (1) a flow module and (2) a sediment transport module. For a complete mathematical description we refer to *WL|Delft Hydraulics* [2003].

[11] The flow module computes flow characteristics (such as water depth, flow velocities and directions, turbulence characteristics) dynamically in time over a three-dimensional computational grid. The flow computations are based on a finite difference solution of the three-dimensional shallow-water equations with a k-ε turbulence closure model [e.g., *Rodi*, 1980]. Bottom friction is modeled on the basis of a user-specified bottom roughness height. A flooding and drying algorithm is used, which includes a grid cell in the computations when the water depth exceeds a certain threshold (0.02 m) and excludes a grid cell when the water depth drops below half this threshold.

[12] The novel aspect of this flow model is that it explicitly accounts for the three-dimensional influence of rigid cylindrical plant structures on (1) drag and (2) turbu-

lence. The influence of the vegetation on drag leads in the momentum equations to an extra source term of friction force, F(z) (N m^{-3}), caused by cylindrical plant structures,

$$F(z) = \frac{1}{2}\rho_0 \phi(z)\, n(z)\, |u(z)|\, u(z), \tag{1}$$

where ρ_0 = the fluid density (kg. m^{-3}); $\phi(z)$ = the diameter of cylindrical plant structures (m) at height, z, above the bottom; n(z) = the number of plant structures per unit area (m^{-2}) at height z; u(z) = the horizontal flow velocity (m s^{-1}) at height z. The influence of the vegetation on turbulence leads in the k-ε equations [e.g., *Rodi*, 1980] to an extra source term of turbulent kinetic energy, k (m^2 s^{-2}), generated by cylindrical plant structures,

$$\left(\frac{\partial k}{\partial t}\right)_{plants} = \frac{1}{1 - A_p(z)} \frac{\partial}{\partial z}\left\{ (1 - A_p(z))(\nu + \nu_T/\sigma_k)\frac{\partial k}{\partial z}\right\} + T(z), \tag{2}$$

where $A_p(z) = (\pi/4)\,\phi^2(z)\, n(z)$ = the horizontal cross-sectional plant area per unit area at height z; ν = the molecular fluid viscosity (m^2 s^{-1}); ν_T = the eddy viscosity (m^2 s^{-1}); σ_k = the turbulent Prandtl-Schmidt number for self-mixing of turbulence ($\sigma_k = 1$); T(z) = F(z)u(z)/ρ_0 = the work spent by the fluid (m^2 s^{-3}) at height z; and an extra source term of turbulent energy dissipation, ε (m^2 s^{-3}), caused by cylindrical plant structures,

$$\left(\frac{\partial \varepsilon}{\partial t}\right)_{plants} = \frac{1}{1 - A_p(z)} \frac{\partial}{\partial z}\left\{ (1 - A_p(z))(\nu + \nu_T/\sigma_\varepsilon)\frac{\partial \varepsilon}{\partial z}\right\} + T(z)\tau_\varepsilon^{-1}, \tag{3}$$

where σ_ε = the turbulent Prandtl-Schmidt number for mixing of small-scale vorticity ($\sigma_\varepsilon = 1.3$); τ_ε = the minimum of the dissipation timescale of free turbulence,

$$\tau_{free} = \frac{1}{c_{2\varepsilon}}\left(\frac{k}{\varepsilon}\right) \tag{4}$$

with coefficient $c_{2\varepsilon} = 1.96$, and the dissipation timescale of eddies in between the plants,

$$\tau_{veg} = \frac{1}{c_{2\varepsilon}\sqrt{c_\mu}}\left(\frac{L^2}{T}\right)^{1/3} \tag{5}$$

with coefficient $c_\mu = 0.09$, where the eddies have a typical size limited by the smallest distance in between the stems,

$$L(z) = C_l\left\{\frac{1 - A_p(z)}{n(z)}\right\}^{\frac{1}{2}}, \tag{6}$$

where C_l = a coefficient reducing the geometrical length scale to the typical volume averaged turbulence length scale. For vegetation, $C_l = 0.8$ was found applicable [*Uittenbogaard*, 2003]. For more details on the k-ε turbulence model, see, for example, *Rodi* [1980]. This plant-flow interaction model has been validated extensively against laboratory flume experiments [e.g., *Baptist*, 2003; *Uittenbogaard*, 2003].

[13] The sediment transport module computes suspended sediment concentrations and sedimentation rates for each time step and each grid cell, on the basis of the three-dimensional advection-diffusion equation for suspended sediment,

$$\frac{\partial C}{\partial t} + \frac{\partial uC}{\partial x} + \frac{\partial vC}{\partial y} + \frac{\partial (w - w_s)C}{\partial z} = \frac{\partial}{\partial x}\left(\varepsilon_{s,x}\frac{\partial C}{\partial x}\right) + \frac{\partial}{\partial y}\left(\varepsilon_{s,y}\frac{\partial C}{\partial y}\right) + \frac{\partial}{\partial z}\left(\varepsilon_{s,z}\frac{\partial C}{\partial z}\right), \tag{7}$$

where C = suspended sediment concentration (kg m^{-3}); u, v and w = flow velocity components (m s^{-1}) in x, y and z directions; $\varepsilon_{s,x}$, $\varepsilon_{s,y}$ and $\varepsilon_{s,z}$ = eddy diffusivities (m^2 s^{-1}) in x, y and z directions; w_s = settling velocity (m s^{-1}) of suspended sediment. The local flow velocities and eddy diffusivities are based on the results of the flow model. The concentration and settling velocity of the suspended sediment at the open boundary of the grid are user-specified for five different sediment fractions.

[14] In accordance with existing tidal marsh models [e.g., *Mudd et al.*, 2004], we only consider the deposition of cohesive suspended sediment from the flooding water, while bed erosion is ignored. These assumptions are realistic for vegetated marsh platforms and for single-tide simulations, as presented here. Field studies have shown that hydrodynamic forces, during flooding of a vegetated marsh platform, are typically too weak to cause erosion [e.g., *Christiansen et al.*, 2000; *Wang et al.*, 1993]. It was not the aim of this study to simulate tidal channel evolution or morphodynamics over longer time periods (including storms), which would necessitate to include channel erosion [e.g., *Fagherazzi and Furbish*, 2001; *Fagherazzi and Sun*, 2004] and waves causing erosion at the mudflat-marsh edge.

[15] The sedimentation rate is traditionally calculated using the Partheniades-Krone formulation [*Partheniades*, 1965],

$$SR = w_s C_b\left(1 - \frac{\tau}{\tau_{cr,d}}\right) \quad \tau < \tau_{cr,d}$$
$$SR = 0 \quad \tau \geq \tau_{cr,d}, \tag{8}$$

where SR = the sedimentation rate (kg m^{-2} s^{-1}); C_b = the suspended sediment concentration (kg m^{-3}) in the computational layer just above the bottom; τ = the bottom shear stress (N m^{-2}) computed by the hydrodynamic model; $\tau_{cr,d}$ = the user-specified critical shear stress for sediment deposition (N m^{-2}).

[16] The flow and sediment transport model were applied on an orthogonal rectangular grid representing the study area, with a horizontal resolution of 2 by 2 m (Figure 1c). In the vertical dimension, eight layers were used in a so-called σ co-ordinate system [*Philips*, 1957]. A time step of 3 s was used, so that numerically stable simulations were obtained. The model was run for single tidal cycles.

3.2. Field Data for Model Input, Calibration, and Validation

[17] Below, we explain how the following field data were collected (Table 1). For the flow model, input data were

Table 1. Overview of Model Input Variables and Their Input Values That Were Used for Different Series of Model Runs[a]

Variable	Calibration		Validation		Simulation of Influence of Variables			
	Flow	Sed	Flow	Sed	hw	H	n	Z
$Z(x, y)$	Figure 1c	Figure 1c	Figure 1c	Figure 1c	Figure 1c	Figure 1c	Figure 1c	flat
$H(x, y)$	Figure 1d + 2a	Figure 1d + 2a	Figure 1d + 2a	Figure 1d + 2a	Figure 1d + 2a	0:15:60	Figure 1d + 2	Figure 1d + 2a
$n(x, y, z)$	Figure 1d + 2a	Figure 1d + 2a	Figure 1d + 2a	Figure 1d + 2a	Figure 1d + 2a	Figure 1d + 2a	0:5:100	Figure 1d + 2a
$\Phi(x, y, z)$	Figure 1d + 2a	Figure 1d + 2a	Figure 1d + 2a	Figure 1d + 2a	Figure 1d + 2a	Figure 1d + 2a	Figure 1d + 2a	Figure 1d + 2a
hw	2.78	2.78	2:0.5:3	2:0.5:3	2:0.1:3.4	2:0.1:3.4	2:0.1:3.4	2:0.1:3.4
$h_i(t)$	Figure 2b	Figure 2b	Figure 2b	Figure 2b	Figure 2b	Figure 2b	Figure 2b	Figure 2b
$C_i(t)$	...	Figure 2b	...	Figure 2b	Figure 2b	Figure 2b	Figure 2b	Figure 2b
z_0	1:1:10	6	6	6	6	6	6	6
ν_h	1:1:30	5	5	5	5	5	5	5
$w_{s,50}$	...	1:1:10	...	4	4	4	4	4
$\tau_{cr.d}$	...	1:1:30	...	5	5	5	5	5

[a]Each model run is a simulation of one single inundation cycle. Notation: flow, flow model run; sed, sedimentation model run; Z, bottom elevation (m NAP); H, vegetation height (10^{-2} m); n, vegetation density (% relative to measured density in the field); ϕ, diameter of plant structures (meters); hw, high water level (m NAP); $h_i(t)$, time series of water level (m NAP) at seaward open boundary; $C_i(t)$, time series of suspended sediment concentration (kg m^{-3}) at seaward open boundary; z_0, bottom roughness height (10^{-3} m); ν_H, horizontal eddy viscosity (10^{-4} m^2 s^{-1}); $w_{s,50}$, median settling velocity of suspended sediment (10^{-4} m s^{-1}); $\tau_{cr,d}$, critical shear stress for sediment deposition (10^{-2} N m^{-2}). Variables may vary in horizontal directions (x,y), vertical direction (z), and with time (t). For space- or time-varying variables, we refer to the figures where the data are plotted. The notation a:b:c means that different values were used ranging from a to c in steps of b.

collected on (1) topography, (2) vegetation characteristics, and (3) temporal water level changes at the seaward open boundary of the study area (Figures 1c and 1d). The output of the flow model (i.e., flow velocities and directions over the study area) was calibrated and validated against field measurements of flow velocities and directions at locations 1, 2 and 3 (Figure 1c). For the sediment transport model, input data were collected on suspended sediment concentrations at the seaward open boundary of the study area. The output of the sediment transport model (i.e., the spatial sedimentation pattern over the study area) was calibrated and validated against field measurements of sedimentation rates at 50 locations randomly distributed over the study area (Figure 1c). The field measurements of flow velocities and the spatial sedimentation pattern have been described in detail by *Temmerman et al.* [2005].

3.2.1. Topography

[18] Elevation data were obtained from airborne laser altimetry carried out in 2001 (Rijkswaterstaat, Meetkundige Dienst), with a resolution of 3 by 3 m, a horizontal accuracy of 0.2 m and vertical accuracy of 0.13 m (corrected for laser reflection on the marsh vegetation) [*Temmerman et al.*, 2005]. The elevation data were interpolated to the 2 by 2 m computational grid, resulting in a detailed and smooth representation of the marsh topography, except for the tidal creeks, because the resolution of the grid (2 by 2 m) was too low to capture all the details of the creek network (creek widths range from 0.3 to 7 m in the study area). Increasing the grid resolution would considerably increase the computation time and was not found to be appropriate. Instead, creeks smaller than $^1\!/_2$ of the grid resolution were not represented in the grid (i.e., creeks <1 m wide, total length = 76 m). For all other creeks, the creek width was adjusted so that at least one grid cell of 2 by 2 m was contained within every creek cross section. For these creeks, elevation values were interpolated to the grid from field survey data of the thalweg of the creeks, so that a smooth, continuous representation of the creek topography was obtained (see Figure 1c).

3.2.2. Vegetation

[19] As input for the plant-flow interaction model, we need to know the average diameter, $\phi(z)$, and the number,

n(z), of cylindrical plant structures (stems and leaves) per unit area in the horizontal plane, at different heights, z, above the bottom (see equations (1) to (6)). The horizontal variation of $\phi(z)$ and n(z) was defined by assigning a certain vegetation type to each grid cell, on the basis of a vegetation map of the study area [*Koppejan*, 2000] (Figure 1d). The vegetation types consist of a combination of four dominant plant species (Table 2). For each of these four species, $\phi(z)$ and n(z) were determined by harvesting the aboveground plant material from two replicate 50 by 50 cm plots in vertical layers of 0.1 m height. For the stems, $\phi(z)$ and n(z) were measured in each vertical layer. For the leaves, the total frontal surface area, a(z), was measured in each layer using an LED scanner. The model assumes that all plant structures, including the leaves, are cylindrical. Therefore, as an approximation, we assumed that the leaves are cylindrical, with a diameter, $\phi(z)$, that is equal to the stem diameter in that layer, and with a total number of leaves, calculated as a(z)/$\phi(z)$. Finally, n(z) and $\phi(z)$ could be calculated for each vegetation type, on the basis of the percentage of the four dominant plant species in each vegetation type (Figure 2a and Table 2).

3.2.3. Boundary Conditions

[20] At the seaward open boundary of the grid (Figure 1c), a time series of tidal water level needed to be specified as input for the flow model, and a time series of suspended sediment concentration (SSC) as input for the sediment transport model. Both time series were based on field data measured at location 1 (Figure 2b) from June to October 2002, using a pressure sensor measuring water level changes (in m relative to Dutch ordnance level, NAP), and an optical backscatter sensor (OBS) measuring turbidity (in FTU = Formazine Turbidity Units). FTU values were calibrated to SSC values (in g L^{-1}), on the basis of a correlation between the OBS signal (in FTU) and SSC (in g L^{-1}) determined from 32 water samples ($R^2 = 0.91$). Simulations were run for individual semi-diurnal tidal cycles, starting just before flooding and ending just after complete drainage of the study area.

[21] All other boundaries of the grid were delineated from aerial photographs in the middle between the studied creek catchment and adjacent catchments (Figure 1c). It is

Table 2. Percentage of Dominant Plant Species in Each Vegetation Type in the Study Area[a]

	Kp10	Kp26	Kp17	Kp21	Kp53	Kp70	Km63	Km100	Km89	Km86	Km92
b.s.	80	60	10	10							
S.a.	20	40	90	90	100	70					
P.m.							60	75	15		
H.p.						30	40		85	100	100
L.v.								25			

[a]Plant species: b.s., bare soil; S.a., *Spartina anglica*; P.m., *Puccinellia maritima*; H.p., *Halimione portulacoides*; L.v., *Limonium vulgare*. Note that vegetation types near the mudflat-marsh edge (Figure 1) include patches with bare soil. Data after *Koppejan* [2000].

assumed that these catchment boundaries are closed boundaries. This assumption is supported by water and sediment balances, which were computed from field measurements and which indicated that fluxes between the studied creek catchment and adjacent catchments are minimal [*Temmerman et al.*, 2005].

3.2.4. Model Calibration and Validation Against Field Data

[22] The model output was calibrated against field data collected for the semi-diurnal inundation cycle of 11 August 2002, which was a high spring tide (high water level about 0.5 m above the high marsh platform). The remaining model variables, for which no input values could be determined from field data, were used for model calibration (see Table 1).

[23] First, the flow model was calibrated against hydrodynamic data (water level, flow velocities and directions) measured at locations 1, 2 and 3 (Figure 1c), using pressure sensors and bidirectional electro-magnetic flowmeters (EMF) at 7 cm above the bottom. The bottom roughness height, z_0, and horizontal eddy viscosity, ν_H, were used as calibration variables. A series of simulations were run using different combinations of z_0 and ν_H values (Table 1). Optimal values for both variables were defined by comparison of simulated and observed time series (5-min intervals) of flow velocities at location 2 in the creek system (Figure 1c). This location was used because flow velocity variations in a tidal creek are a simple but reliable measure

for the overall spatial flow pattern in the corresponding marsh creek catchment. They allow calculation of the relative importance of flow via the creek system versus flow via the seaward marsh edge to the marsh platform [*Temmerman et al.*, 2005]. In order to determine the optimal z_0 and ν_H values, the model efficiency coefficient, ME, was calculated for each run as [*Nash and Sutcliffe*, 1970]

$$ME = 1 - \frac{\sum(OBS - SIM)^2}{\sum(OBS - MEAN)^2}, \qquad (9)$$

where OBS is the observed flow velocity, SIM is the simulated flow velocity, and MEAN is the mean of the observed flow velocities. Values for ME range from $-\infty$ to 1. The closer ME approximates 1, the better the model simulates individual observations.

[24] Secondly, the sedimentation model was calibrated against the observed spatial sedimentation pattern. This was measured using filter paper sediment traps (diameter = 0.15 m; pore diameter = 0.45 μm) at 50 locations in the study area (Figure 1c). The filter papers were attached to aluminium plates and fixed to the marsh surface just before and collected after tidal inundation. Subsequently, the filter papers were washed to remove salts, oven-dried for 24 hours at 50°C and reweighed to determine the sedimentation rate (in g m^{-2} per tide). The settling velocity, w_s, and critical shear stress for sediment deposition, $\tau_{cr,d}$, were used as
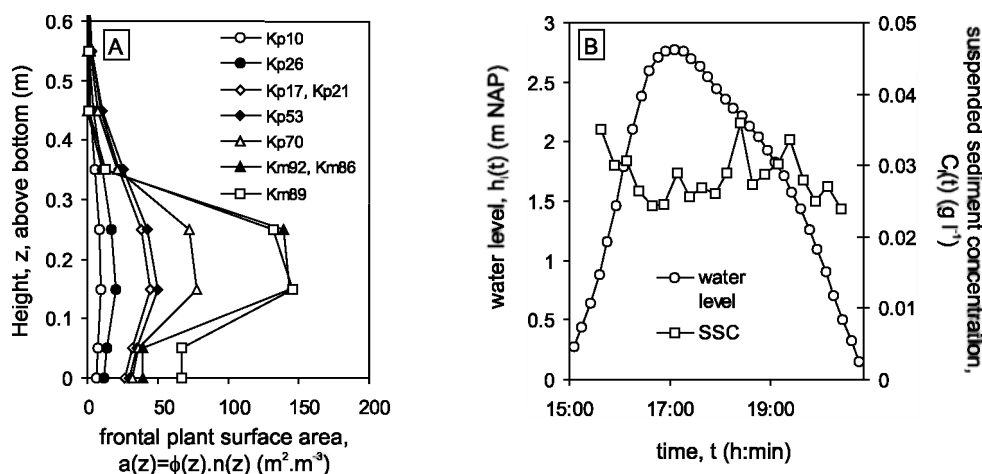

Figure 2. Model input data. (a) Vertical plant structure for the different vegetation types in the study area: a(z), frontal plant surface area (m^2 m^{-3}) at height, z, above the bottom; φ(z), diameter of plant structures (m) at height z; n(z), number of plant structures per m^2 at height z. Vegetation types vary in space (see Figure 1c) and are specified in Table 2. (b) Time series of water level, $h_i(t)$ (m NAP), and of suspended sediment concentration, $C_i(t)$ (kg m^{-3}), at the seaward open boundary of the model grid.

calibration variables. The settling velocity, w_s, was defined for five different suspended sediment classes at the open boundary of the grid. One $\tau_{cr,d}$ value was defined over the whole grid. The distribution of settling velocities over the five sediment classes was based on data on the grain size distribution of suspended sediments, which were sampled in the study area at the marsh edge [*Chen et al.*, 2005]. These grain size analyses were performed on dispersed sediments, while in situ flocculation is important and will increase the settling velocity. We assumed that the sorting, skewness and kurtosis of the settling velocity distribution was the same as for the dispersed grain size distribution. Under this assumption, only the median settling velocity, $w_{s,50}$, remains unknown and was used as a calibration variable. Similar to the calibration of the flow model, simulations were run for different combinations of $w_{s,50}$ and $\tau_{cr,d}$ values (Table 1). Optimal values for both parameters were determined by comparison of simulated and observed sedimentation rates at the 50 sediment trap locations (Figure 1c) using the model efficiency coefficient (equation (9)).

[25] After model calibration for the inundation cycle of 11 August 2002, the model was run and validated for a series of other inundation cycles (see Table 1). First, the flow model was validated for inundations ranging from neap to spring tides with high water levels ranging from 2 to 3 m NAP. For these tides, measured and simulated flow velocities were compared in the creek (location 2) and on the vegetated marsh platform (location 3) (Figure 1c). The detailed spatial pattern of flow velocities and directions, which was simulated for these inundations, was not measured in the field and therefore could not be directly validated against field data. However, an integrative validation was performed for the high marsh platform, on the basis of the percentage of water, $V_{creek,\%}$, that flowed to and from the high marsh via the tidal creek system, calculated as

$$V_{creek,\%} = \left(\frac{V_{creek}}{V_{total}} \right) \cdot 100, \tag{10}$$

where V_{creek} = the water volume transported through the creek system (at location 2), and V_{total} = the total water volume above the corresponding creek catchment (i.e., the high marsh) at the moment of high tide. V_{creek} was calculated on the basis of the measured and simulated flow velocities, water level variations and creek cross-section at location 2. V_{total} was calculated by assuming a flat water surface at high tide and calculating the water volume at high tide above the marsh surface, on the basis of the digital elevation map of the studied creek catchment (Figure 1c). Values of $V_{creek,\%}$ provide a simple measure for the spatial flow pattern: when the spatial flow pattern is characterized by flow perpendicular to the creeks, $V_{creek,\%}$ = 100% (i.e., all water is supplied to and drained from the marsh platform via the creek system), whereas flow perpendicular to the marsh edge is reflected by $V_{creek,\%}$ = 0% (i.e., all water passes via the marsh edge and not via the creek system). In practice, $V_{creek,\%}$ values will vary between 0 and 100% and in this way reflect the relative importance of flow perpendicular to the creeks versus flow perpendicular to the marsh edge. Values of $V_{creek,\%}$ were calculated from measurements and simulations for inundation cycles ranging from neap to spring tides (see Table 1). Finally, the

sedimentation model was validated for three spring tidal cycles, during which sedimentation rates were measured at 50 locations, as explained above.

3.3. Simulating and Quantifying the Relative Influence of Controlling Factors

[26] Once calibrated and validated, the model was used to study the influence of a number of factors, which are thought to control flow hydrodynamics and sedimentation rates on tidal marshes (Table 1). First, the influence of high water level was investigated by simulating tidal inundation cycles with different high water levels. Secondly, for each of these tidal cycles with a different high water level, the influence of (1) the vegetation density and height, and (2) the micro-topography of the high marsh platform was simulated. The ranges of input values that were used for these variables are summarized in Table 1.

[27] The impact on the simulated flow and sedimentation patterns was evaluated as follows. In order to avoid the visual comparison of a large amount of spatial maps of flow vectors and sedimentation rates, we defined simple measures to characterize the spatial flow and sedimentation patterns, so that these measures could be plotted against the controlling variables in simple scatterplots. The spatial flow pattern was characterized by $V_{creek,\%}$, as described above (equation (10)). The spatial sedimentation pattern on tidal marshes can be characterized using a regression model [*Temmerman et al.*, 2005, 2003],

$$SR = k \cdot e^{lH} \cdot e^{mD_c} \cdot e^{nD_e}, \tag{11}$$

where SR = the sedimentation rate (g m^{-2}), H = the elevation of the marsh surface (m relative to a certain reference level, here the Dutch ordnance level NAP), D_c = distance from the nearest tidal creek (m), and D_e = distance from the seaward marsh edge, measured along the nearest creek (m). Here k, l, m and n are regression parameters for which k > 0 and l, m, n < 0. For each simulated inundation cycle, the sedimentation rates computed in each grid cell of the vegetated marsh surface were related to the corresponding H, D_c and D_e values using this regression model. The obtained regression parameters are a good measure then to characterize the spatial sedimentation pattern. The regression parameter k is a measure for the overall amount of deposited sediment; highly negative l values reflect a rapid decrease of sedimentation rates with increasing elevation, H; highly negative m values reflect a rapid decrease of sedimentation rates with increasing distance from creeks, D_c; and highly negative n values reflect a rapid decrease of sedimentation rates with increasing distance from the marsh edge, D_e.

4. Results

4.1. Model Calibration, Validation, and Analysis

[28] The calibration of the flow model against flow velocities measured in the creek (location 2) resulted in an optimal z_0 value of 0.006 m and optimal ν_H value of 0.0005 m^2 s^{-1}. For these z_0 and ν_H values the best correspondence between observed and simulated creek flow velocities was obtained (Table 3 and Figure 3). Using these optimal z_0 and ν_H values, the validation runs also resulted in

Table 3. Summary of Model Calibration and Validation[a]

| | Calibration | | Validation | | | | | |
| | Tide 1 | | Tide 2 | | Tide 3 | | Tide 4 | |
	ME	R^2	ME	R^2	ME	R^2	ME	R^2
Creek flow (location 2)	0.86	0.91	0.76	0.80	0.80	0.88	0.75	0.81
Vegetation flow (location 3)	0.53	0.64	0.54	0.56	0.49	0.55	0.55	0.68
Sedimentation pattern	0.56	0.65	0.65	0.72	0.59	0.67	0.53	0.61

[a]ME (i.e., model efficiency coefficient, equation (9)) and R^2 values are given for observed versus simulated (1) creek flow (i.e., time series of flow velocity in the creek at location 2 in Figure 1c), (2) vegetation flow (i.e., time series of flow velocity in the marsh vegetation at location 3), (3) sedimentation pattern (i.e., sedimentation rates measured at 50 locations). Tide 1 (11 August 2002) was used for calibration, tides 2, 3 and 4 (12 August, 10 September, and 11 September 2002) were used for validation.

a good correspondence between observed and predicted creek flow velocities (Table 3). As reported from many other tidal marsh creeks, our field measurements showed that peaks in the creek flow velocity typically occur at the moment of flooding and drainage of the surrounding marsh platform (Figure 3). These velocity pulses were also simulated fairly well by the model (Figure 3). The model underestimated, however, the measured creek ebb velocities. This may be attributed to the drying algorithm, which excluded grid cells from the computations once the water depth felt below 0.01 m. Consequently, small amounts of water are kept in the cells on the marsh platform and do not drain to the creeks, causing the underestimated creek ebb velocities. In addition, the deletion of creeks smaller than 1 m wide form the grid (see above) may lead to poorer drainage of the marsh platform as compared to the field situation.

[29] The flow velocities that were simulated on the vegetated marsh platform (location 3) correspond reasonably well with the field measurements (Table 3). The model

simulations show that the vertical flow profile changes with time, as the water level changes from within to above the vegetation canopy during an inundation cycle (Figure 4). On the vegetated marsh platform (e.g., location 4, Figure 1c), we can distinguish two vertical zones (Figure 4a): (1) within the vegetation canopy, flow velocities are reduced owing to friction; and (2) once the water level exceeds the height of the vegetation canopy, maximum flow velocities are simulated above the canopy. Vertical variations in flow direction are negligible within the vegetation canopy, but small differences in flow direction are simulated between the zones within and above the canopy (Figure 4a). At the edge between the unvegetated mudflat and vegetated marsh (location 5, Figure 1c), larger differences in flow direction and more complex velocity variations are simulated over the vertical profile (Figure 4b).

[30] At a larger scale, the spatial patterns of flow velocities and directions also change during an inundation cycle (Figure 5). First, the mudflat in front of the low marsh is flooded from the seaward open boundary by a uniform landward sheet flow, with flow velocities around 0.07 m s^{-1} (Figure 5a). As this uniform sheet flow arrives at the irregular edge between the unvegetated mudflat and vegetated low marsh, flow velocities are reduced within the vegetation ($\sim$0.04 m s^{-1}), while velocities are enhanced in between vegetated areas (up to 0.15 m s^{-1}) (Figures 5a and 5b). Furthermore, flow directions converge in between the vegetated areas, indicating that the water flows preferentially over unvegetated surfaces (where friction is lowest) instead of through the vegetation. As the water level further rises above the top of the vegetation canopy, an increasing vertical variation in flow patterns is simulated (Figures 4b, 5c, and 5d). Near the bottom (below the top of the vegetation canopy), flow velocities are reduced within the vegetation and enhanced in between vegetated areas (i.e., the flow pattern as described above) (Figure 5c). In contrast, near the water surface (above the top of the
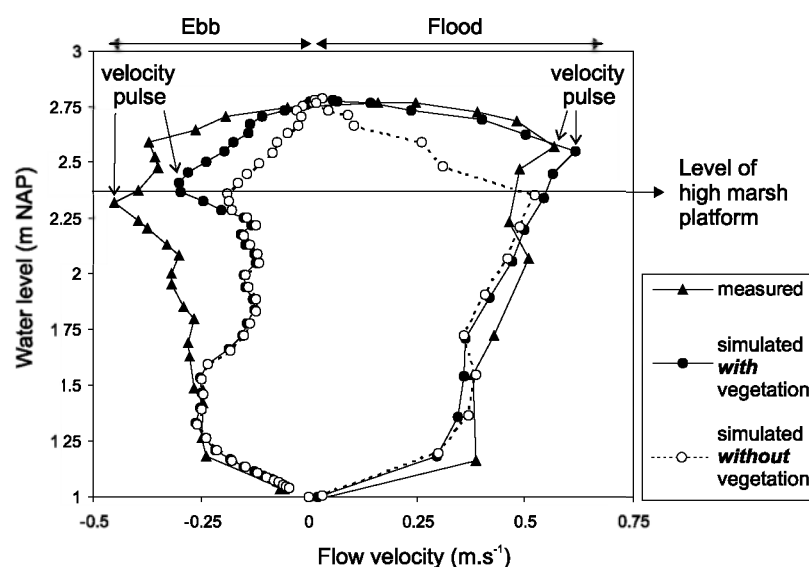

Figure 3. Water level versus flow velocity in the creek at location 2 (see Figure 1) during one tidal inundation cycle (11 August 2002): comparison of measurements and simulations with and without vegetated marsh platform. Note the velocity pulses around the moment of flooding and drainage of the marsh platform.
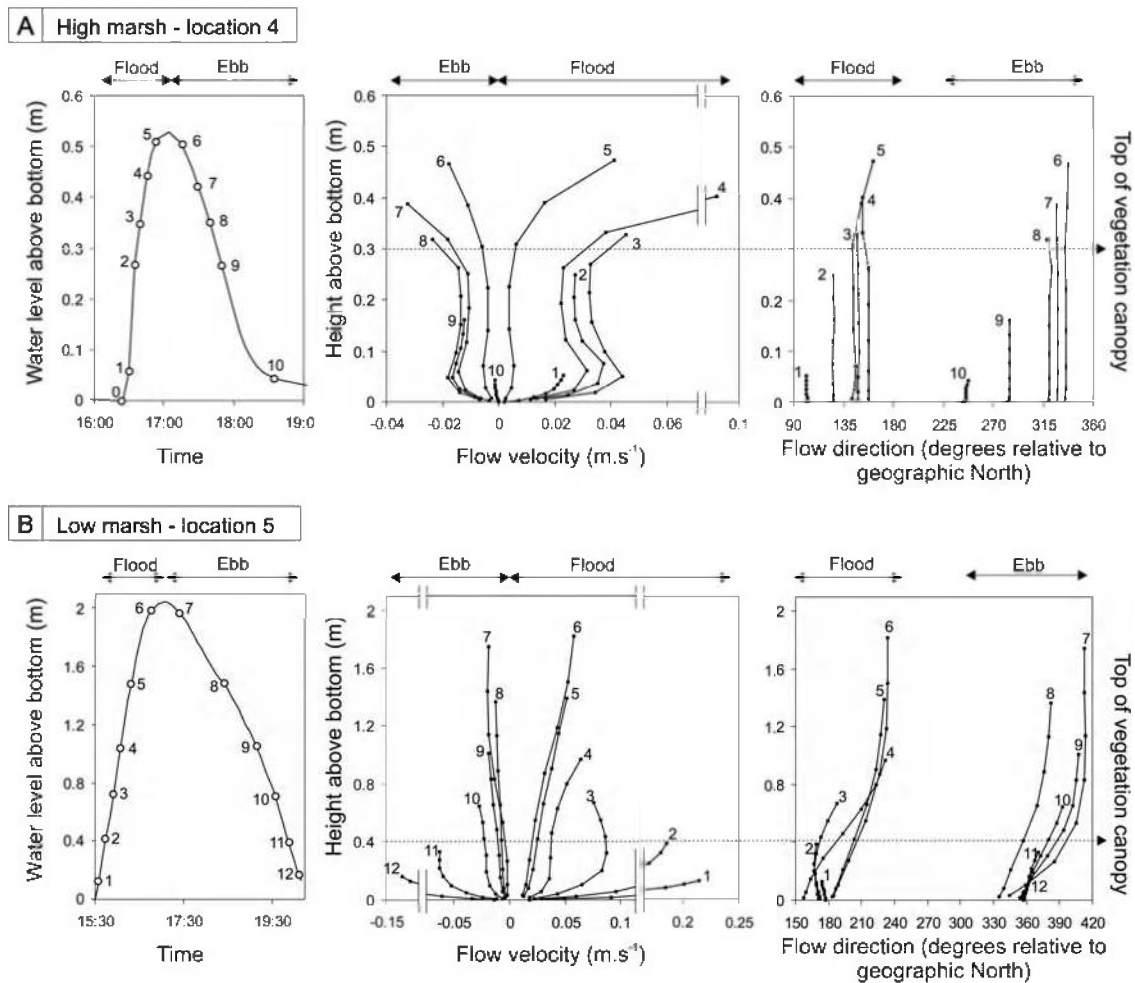
Figure 4. Simulated vertical profiles of flow velocity and flow direction during an inundation cycle (11 August 2002) (a) at the edge between the low marsh and mudflat (location 5, see Figure 1) and (b) above the high marsh platform (location 4). Vertical profiles are shown for successive time steps (indicated by numbers) during the inundation cycle.

vegetation canopy) quasi uniform landward sheet flow is simulated (Figure 5d). This flow pattern on the low marsh persists during the rest of the flood.

[31] On the high marsh, which consists of a vegetated platform dissected by unvegetated creeks, the creeks are first flooded at quite high flow velocities ($\sim$0.5 m s^{-1}) (Figure 5e). Once the water level exceeds the level of the creek banks, the creek water starts to flood the high marsh platform, as indicated by flow directions perpendicular to the creeks (Figure 5f). This flooding, starting from the creeks, causes the flow velocity pulses in the creek (Figure 3). The flow velocity above the marsh platform rapidly decreases (to $\sim$0.05 m s^{-1}) as soon as the creek water flows into the marsh vegetation (Figure 5f). As the water level further rises and exceeds the top of the vegetation canopy, the flow directions become more or less perpendicular to the seaward open boundary instead of to the creeks, indicating that large-scale sheet flow via the mudflat-marsh edge becomes more important than flow via the creeks (Figures 5g and 5h). As a consequence, the flow velocities in the creek slow down (Figure 3). Vertical variations in flow patterns are of minor importance above

the high marsh, as the water level overtops the vegetation only close to high tide, when velocities are almost zero (Figure 4a). During the ebb, the reverse flow patterns are simulated, although flow velocities are generally lower than during the flood (Figure 3 and 4).

[32] The simulated spatial flow pattern was validated on the basis of the percentage of water that flowed to and from the high marsh via the tidal creek system, $V_{creek,\%}$ (equation (10)). We first demonstrate that $V_{creek,\%}$ is a good measure to characterize the spatial flow pattern. During a simulated inundation cycle, the creeks are flooded first, which is reflected by $V_{creek,\%} = 100\%$ (Figure 6a). Next, once the high marsh platform starts to flood, flow directions are mainly perpendicular to the creeks, except for a small zone near the marsh edge, where flow directions are perpendicular to the marsh edge (Figure 5f). As a consequence, $V_{creek,\%}$ starts to decrease slowly but still remains rather close to 100% (Figure 6a). Once the water level exceeds the top of the vegetation canopy, flow directions become perpendicular to the marsh edge over almost the whole marsh platform (Figures 5g and 5h), which is reflected by a sudden decrease in $V_{creek,\%}$ (Figure 6a). During the ebb, the reverse
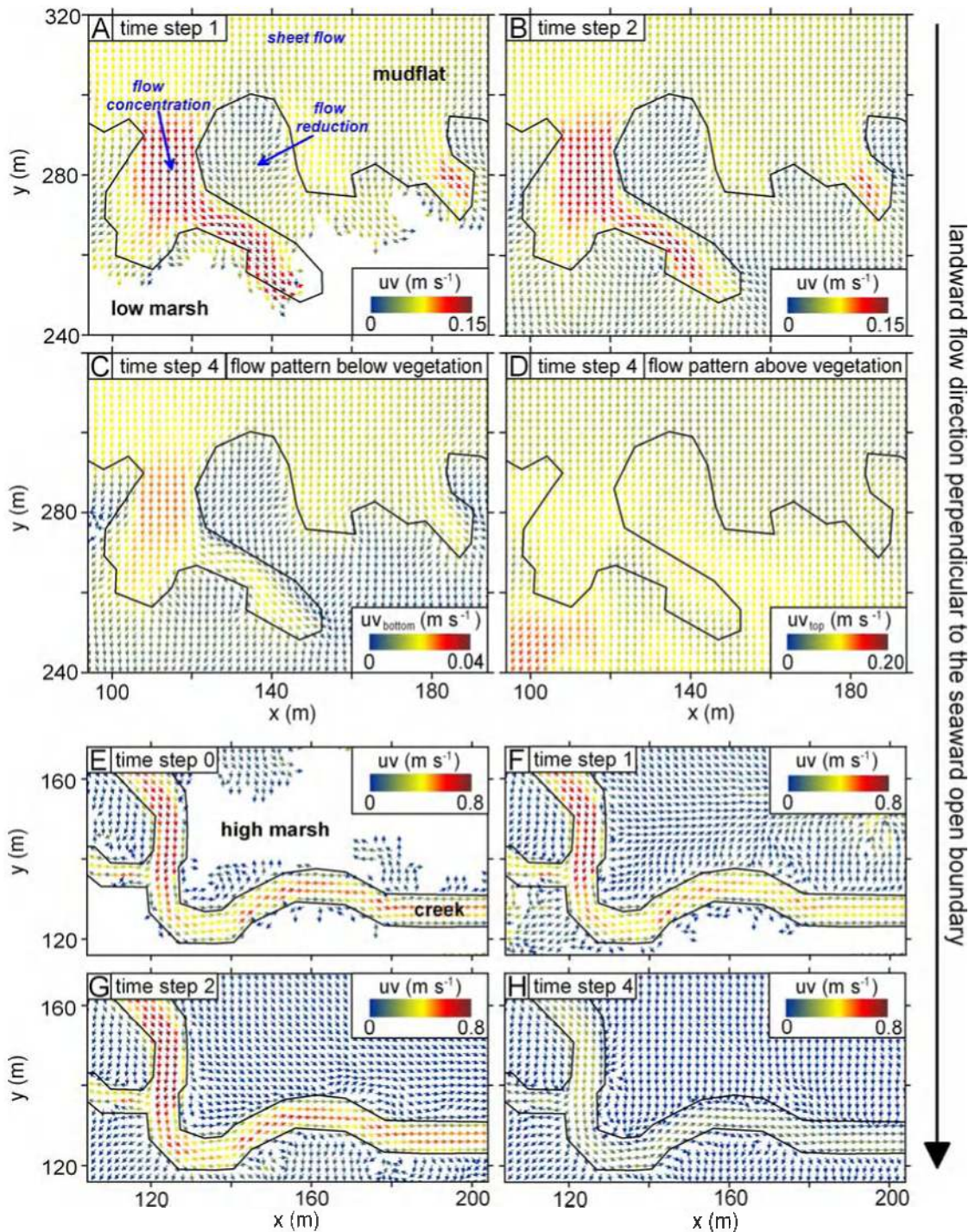
Figure 5. Simulated spatial patterns of flow velocities and directions for selected time steps during one inundation cycle (11 August 2002). (a–d) Detail for the edge between the low marsh and mudflat. Note that Figures 5a and 5b display depth-averaged flow velocities (uv) for different time steps, while Figures 5c and 5d display flow velocities in the bottom layer (uv$_{bottom}$) and top layer (uv$_{top}$) of the water column, respectively, for the same time step. Time steps are indicated on the water level curve on Figure 4b. (e–g) Detail for the high marsh platform, showing depth-averaged flow velocities (uv) for different time steps. Time steps are indicated on Figure 4a.

flow patterns are simulated. When looking at different inundation cycles with different high water levels, V$_{creek,\%}$ follows about the same time trajectory, but V$_{creek,\%}$ at high tide is different for inundation cycles with different high

water levels (Figure 6a). V$_{creek,\%}$ at high tide is then a good measure to characterize the relative importance of flow perpendicular to the creeks versus flow perpendicular to the marsh edge over a whole inundation cycle. Figure 6b
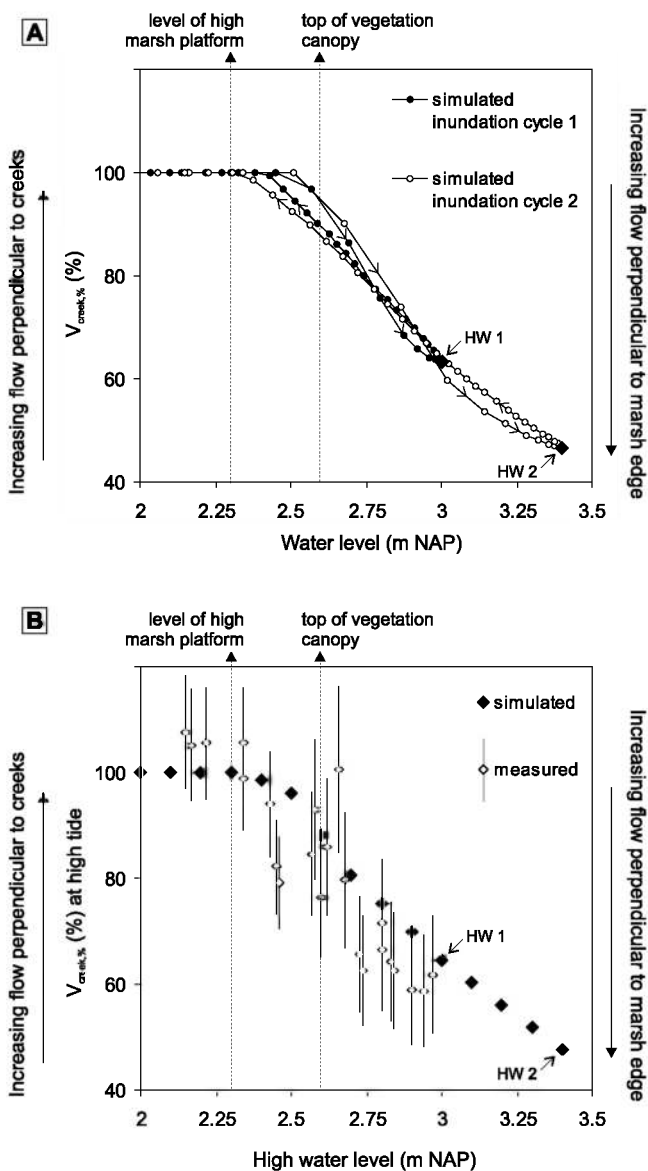
Figure 6. (a) Percentage of water, $V_{creek,\%}$, that flows to and from the high marsh via the tidal creek system versus water level simulated during two single inundation cycles. Each dot represents a 5-min time step; the time trajectory is indicated by arrows. (b) $V_{creek,\%}$ at high tide versus high water level for different inundation cycles: comparison of measured and simulated data. Error bars represent uncertainty on the measured data [see *Temmerman et al.*, 2005]. Each dot represents high tide data for one inundation cycle. For example, the high tide data for two inundation cycles (HW1, HW2) are indicated in both Figures 6a and 6b.

shows that a good correspondence is obtained between $V_{creek,\%}$ at high tide calculated from field measurements (explained above) and from the model simulations. This demonstrates that the model is able to simulate the overall flow pattern via the creeks versus flow via the marsh edge. It further confirms our assumption that water fluxes via the closed boundaries of the creek catchment are negligible.

[33] Finally, the sedimentation model was calibrated and validated against the sedimentation rates measured at 50

locations. This resulted in an optimal $w_{s,50}$ value of 0.0004 m s^{-1} and $\tau_{cr,d}$ value of 0.05 N m^{-2}. Both for the calibration and validation runs, the correspondence between observed and simulated sedimentation rates is reasonably good (Table 3). In agreement with the spatial flow pattern, the field data and model simulations show that sedimentation rates decrease with increasing marsh surface elevation, increasing distance from the marsh edge and increasing distance from creeks (Figures 7 and 8).

4.2. Simulating the Relative Influence of Inundation Height, Vegetation, and Micro-Topography

[34] At the edge of the mudflat and low marsh, the spatial pattern of vegetated and unvegetated areas was found to be fully responsible for the flow and sedimentation pattern. Without vegetation cover, uniform sheet flow occurs in the model and sediment is deposited very homogeneously in space (Figures 8b and 8d). In contrast, if the marsh is (partly) covered by vegetation, the difference in flow resistance between vegetated and unvegetated areas results in faster propagation of the flood wave over the unvegetated surfaces. As a consequence, flow velocities are enhanced and sediment deposition reduced in between vegetated areas, while flow velocities are rapidly reduced and sediment is rapidly deposited within vegetated areas (Figures 8a and 8c).

[35] The presence or absence of a vegetation cover is also crucial on the high marsh. When vegetation is present, flow perpendicular to the creeks is simulated at the beginning of flooding and end of drainage of the high marsh platform (Figure 8e). In contrast, when vegetation is absent, only sheet flow perpendicular to the marsh edge is simulated over the whole inundation cycle (Figure 8f). Related to this, the flow velocity pulses that are observed and simulated in the creek when vegetation is present, completely disappear when an unvegetated marsh is simulated (Figure 3). When vegetation is present, the difference in flow resistance between the unvegetated creeks and vegetated marsh platform results in a faster propagation of the flood wave via the unvegetated creeks, so that the marsh platform is flooded starting from the creeks, leading to the velocity pulse in the creeks and to flow directions perpendicular to the creeks. As a result, sedimentation rates are highest just next to the creeks and decrease rapidly with increasing distance from the creeks, because of sediment trapping along flow paths perpendicular to the creeks (Figure 8g). Without vegetation cover, the propagation of the flood wave is as fast over the marsh platform as via the creeks, so that the marsh platform is flooded starting from the marsh edge, leading to flow directions perpendicular to the marsh edge and no flow velocity pulses in the creeks (Figures 3, 8e, and 8f). As a result, sedimentation rates are (1) lower just next to the creeks (because flow starting from the creeks is negligible), (2) higher at a distance from the creeks (because the sediment is transported and deposited farther onto the marsh) and (3) higher within the creeks (because no velocity pulses occur in the creeks) (Figures 8g and 8h).

[36] A large number of model runs were performed to simulate the relative influence of (1) the high water level of an inundation cycle, (2) the vegetation characteristics (density and height), and (3) the micro-topography of the marsh platform on the spatial flow and sedimentation
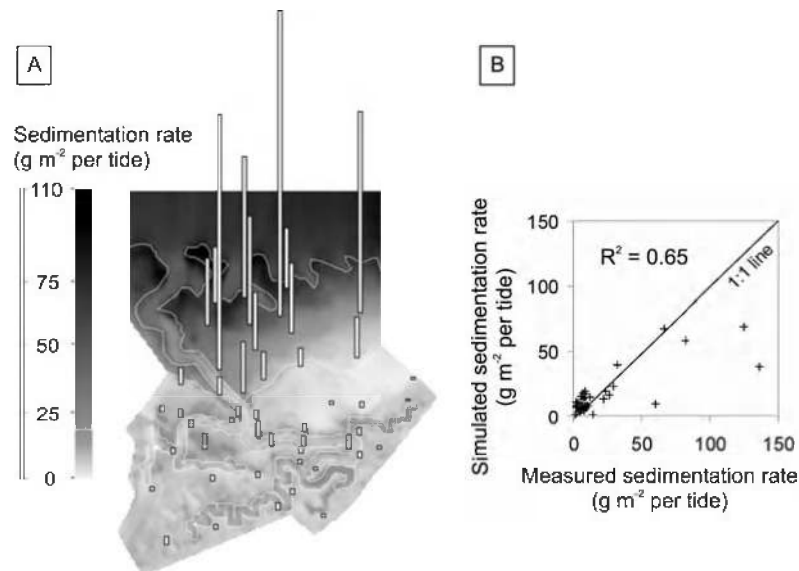
Figure 7. Spatial sedimentation pattern after one tidal inundation cycle (11 August 2002). (a) Comparison of field measurements (bars) and simulated values (gray scale) of sedimentation rate. (b) Scatterplot of measured versus simulated sedimentation rates at the 50 measuring locations.

pattern (Table 1). The flow pattern during an inundation cycle was characterized using $V_{creek,\%}$ at high tide (Figures 9 and 10). As demonstrated above, $V_{creek,\%}$ is a good measure for the spatial flow pattern. The simulated sedimentation pattern was characterized using the regression model in equation (11). For all simulated inundations, the regression model explained more than 85% of the variance of the simulated sedimentation rates, which supports the use of the regression parameters to characterize the simulated spatial sedimentation pattern (Figure 11).

[37] First, both the field measurements and model simulations showed that $V_{creek,\%}$ decreases with increasing high water level (Figure 6b). This may be explained as follows. Flow perpendicular to the creeks (i.e., $V_{creek,\%}$ close to 100%) occurs especially at the beginning of an inundation cycle, when the water level is still below the top of the vegetation canopy (i.e., emergent vegetation) (Figures 5f and 6). During this stage, the flow resistance within the vegetation canopy is much higher than in the unvegetated creeks, so that the flood wave penetrates the marsh faster via the creeks and so that the platform is flooded via the creeks. Once the water level rises above the vegetation canopy (i.e., submerged vegetation), this difference in flow resistance between the creeks and the marsh platform decreases. As a result, sheet flow directly via the marsh edge instead of via the creeks develops and $V_{creek,\%}$ decreases (Figures 5h and 6). During inundation cycles with higher high water levels, this condition with submerged vegetation and sheet flow perpendicular to the marsh edge will take longer. Consequently, $V_{creek,\%}$ at high tide will decrease with increasing high water level (Figure 6b). In accordance with this, the spatial sedimentation pattern changes (Figures 11a–11d): With increasing high water level, the regression parameters l, m and n increase, which means that the sediment is transported higher onto the marsh, farther away from the creeks and from the marsh edge before it is deposited. The

parameter k does not show a clear trend with changing high water level (Figure 11a).

[38] Second, the model runs with different vegetation heights confirm that the relation between $V_{creek,\%}$ and high water level is controlled by the vegetation height (Figures 9a and 9b). They show that for a high inundation with submerged vegetation at high tide, $V_{creek,\%}$ is higher when a higher vegetation canopy is simulated. This is because the period, during which the vegetation is submerged and the flow is perpendicular to the marsh edge, will be shorter when the vegetation is higher. For a shallow inundation with emergent vegetation at high tide, $V_{creek,\%}$ is the same, independent of vegetation height (Figures 9a and 9b). In accordance with this, the spatial sedimentation pattern does not significantly change with vegetation height, for shallow inundations with emergent vegetation (Figures 11e–11h). For high inundations with submerged vegetation at high tide, k increases with increasing vegetation height, which means that more sediment is deposited, and l, m and n decrease, which means that the sediment is deposited more rapidly along its transport pathways from the low to the high marsh, from the creek levees to the basins, and from the marsh edge to the inner marsh (Figures 11e–11h).

[39] Third, with increasing vegetation density, the difference in flow resistance between the unvegetated creeks and vegetated platform will increase, so that flow perpendicular to the creeks will be more important and $V_{creek,\%}$ will increase (Figures 9c and 9d). Furthermore, with increasing vegetation density, more sediment is deposited and the sedimentation difference between low and high marsh, between levees and basins, and between the marsh edge and the inner marsh increases (Figures 11i–11l). The model simulations indicate that the effect of vegetation density is most obvious within the lower range of vegetation densities (0–10%; Figures 9d and 11i–11l). Within the higher range of vegetation densities, the spatial flow and sedimentation
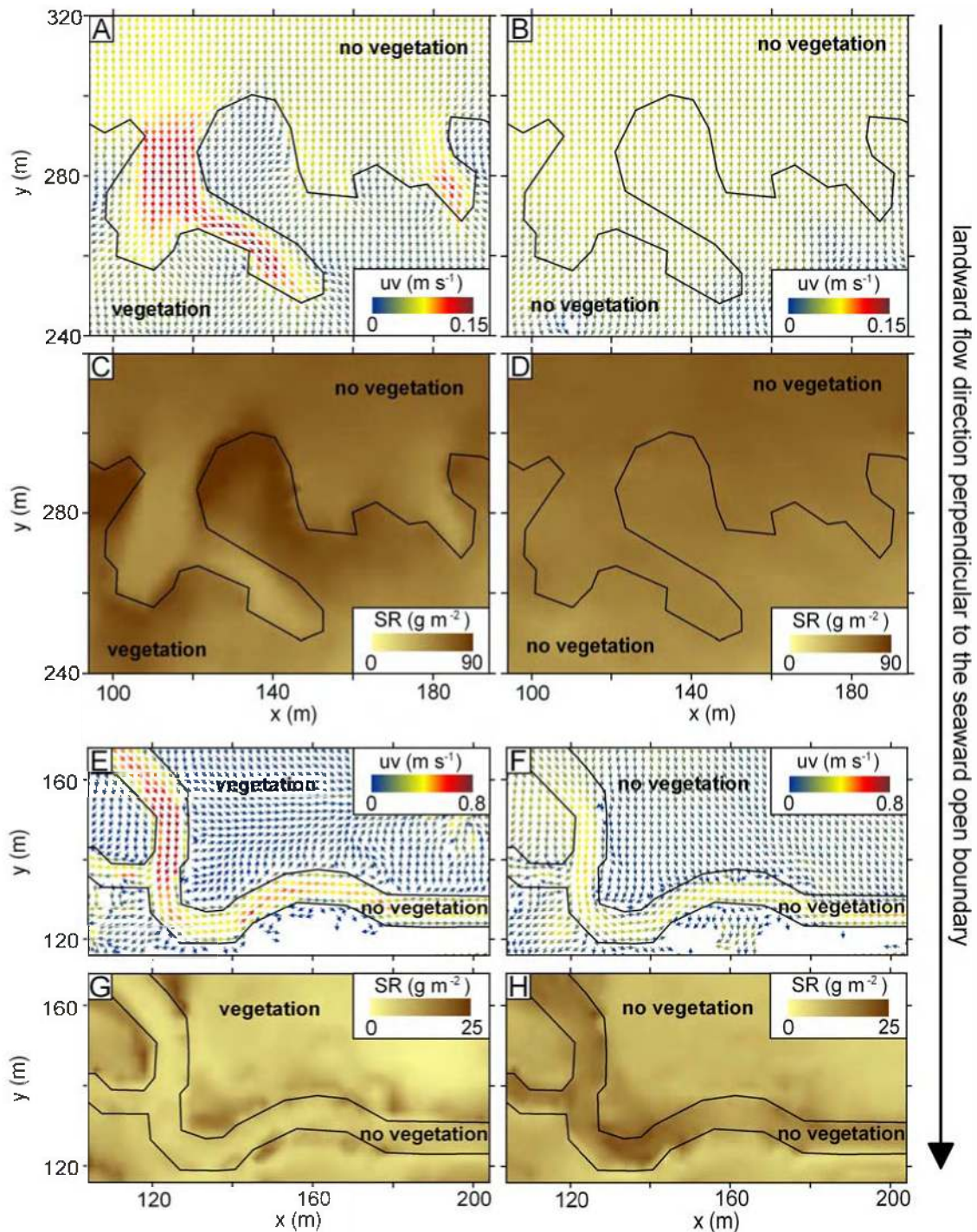
Figure 8. Simulated flow patterns (at the beginning of flooding) and sedimentation patterns (after one inundation cycle) at the edge between the low marsh and mudflat for (a) flow pattern with marsh vegetation and (b) flow pattern without marsh vegetation (uv = depth-averaged flow velocity) and (c) sedimentation pattern with marsh vegetation and (d) sedimentation pattern without marsh vegetation (SR, sedimentation rate). Simulated patterns on the high marsh platform for (e) flow pattern with marsh vegetation and (f) flow pattern without marsh vegetation and (g) sedimentation pattern with marsh vegetation and (h) sedimentation pattern without marsh vegetation.

pattern does not change significantly with changing vegetation density.

[40] Finally, the effect of the micro-topography of the marsh platform is negligible (Figures 10 and 11m–11p). In

the original simulation, the real micro-topography of the marsh platform is used, consisting of levees along the creeks, which are up to 0.3 m higher than basins, at a farther distance from the creeks. However, the use of a flat
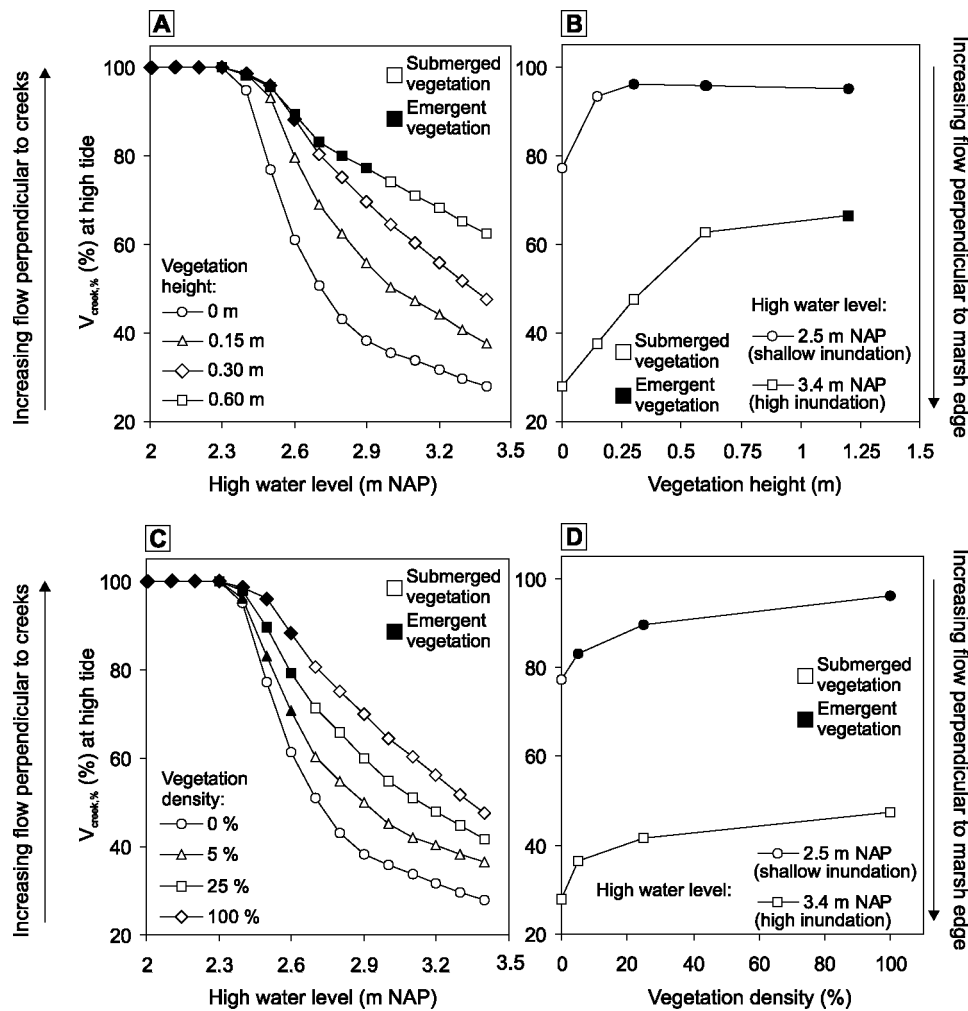
Figure 9. Influence of vegetation characteristics on the simulated spatial flow pattern. (a) $V_{creek,\%}$ at high tide (i.e., percentage of water that flows to and from the high marsh via the tidal creek system) versus high water level for different vegetation heights. (b) $V_{creek,\%}$ versus vegetation height for different high water levels. For Figures 9a and 9b, the real vegetation density, as measured in the field, was used (Figure 2a). (c) $V_{creek,\%}$ at high tide versus high water level for different vegetation densities. (d) $V_{creek,\%}$ versus vegetation density for different high water levels. Here 100% vegetation density is density as observed in the field. For Figures 9c and 9d the real vegetation height, as measured in the field, was used (Figure 2a). Each dot in these graphs represents high tide data for one inundation cycle (compare Figure 6b). Inundation cycles with emergent or submerged vegetation at high tide are indicated in solid or open circles, respectively.

marsh platform, without any micro-topography, does not affect the simulated spatial flow and sedimentation pattern significantly (Figures 10 and 11m–11p).

5. Discussion and Conclusions

[41] Up to now, the influence of vegetation on flow hydrodynamics and sediment transport has been studied in particular on the small scale of a laboratory flume [e.g., *Bouma et al.*, 2005b; *Fischer-Antze et al.*, 2001; *Lopez and Garcia*, 2001; *Nepf and Vivoni*, 2000; *Shi et al.*, 1995] or on the basis of a limited number of point measurements in the field [e.g., *Christiansen et al.*, 2000; *Leonard and Luther*, 1995]. This modeling study gave us a high-resolution, three-dimensional picture of the impact of vegetation on flow hydrodynamics and sediment transport on a landscape scale. It was shown that in a tidal marsh landscape, where topographic gradients are small, the vegetation has the strongest control on flow routing and on the spatial sedimentation pattern during single inundation events, while the influence of the micro-topography is negligible. This implies that the presence or absence of a vegetation cover is determinant for the long-term geomorphology of tidal marshes. Below, these points are discussed.

[42] The model applied here was able to simulate flow and sedimentation patterns that are typically observed in tidal marshes. The model simulated the occurrence of flow velocity pulses in the tidal creeks at the moment of flooding and drainage of the surrounding marsh platform (Figure 3), as widely reported from field measurements in tidal marsh creeks [e.g., *Bayliss-Smith et al.*, 1979; *Bouma et al.*, 2005a; *French and Stoddart*, 1992; *Reed et al.*, 1985]. The simu-
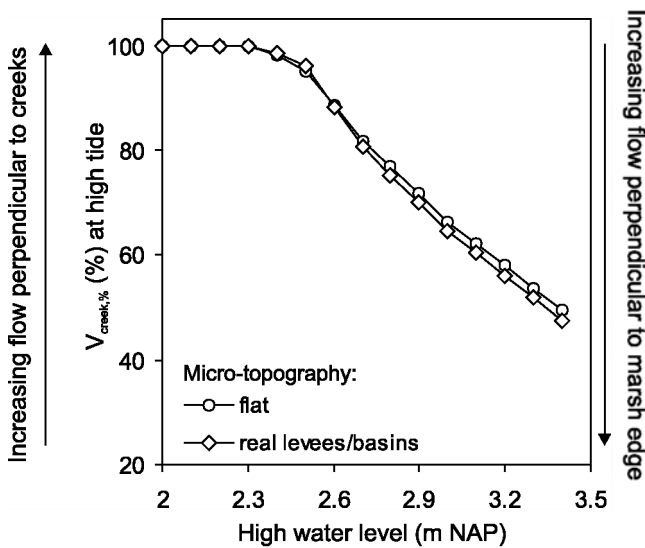
Figure 10. Influence of the micro-topography of the high marsh platform on the simulated spatial flow pattern: $V_{creek,\%}$ at high tide versus high water level for two scenarios of micro-topography, using (1) the real levee-basin topography, as observed in the study area, and (2) a flat topography, without levees and basins. Each circle represents high tide data for one inundation cycle (compare Figure 6b).

lated spatial flow patterns (Figure 5) are in agreement with field studies that showed that flow directions during tidal inundation of a marsh platform vary from perpendicular to tidal channels, at the beginning of flooding and end of drainage of the marsh platform, to parallel to tidal channels, at peak flood and ebb [*Christiansen et al.*, 2000; *Davidson-Arnott et al.*, 2002; *Leonard*, 1997; *Wang et al.*, 1993]. In accordance with field data, the simulations showed that the spatial sedimentation pattern is related to three topographic variables: sedimentation rates decrease with increasing marsh surface elevation, increasing distance from the seaward marsh edge and increasing distance from creeks (Figure 7) [e.g., *French and Spencer*, 1993; *Leonard*, 1997; *Temmerman et al.*, 2003]. In an earlier study, we demonstrated that the spatial sedimentation pattern could be well described using these three topographic variables, ignoring differences in vegetation types [*Temmerman et al.*, 2003]. The present study confirms this but clearly demonstrates that the presence of a vegetation cover is crucial to explain rather than to describe the spatial sedimentation pattern. Until now, this crucial role of vegetation for spatial flow and sedimentation patterns has not been identified from field measurements.

[43] This modeling study showed that the flow patterns in tidal creeks (flow velocity pulses) and on marsh platforms (changing flow directions) are linked to each other and, most importantly, that the presence of a vegetation cover is the key factor controlling these flow and sedimentation patterns (Figures 3 and 8). In contrast, the influence of the micro-topography of the marsh platform is negligible (Figures 9, 10, and 11). It was shown that the vegetation has a three-dimensional effect. In the two horizontal dimensions, frictional differences between vegetated and unvegetated areas will result in preferential flow routing over

unvegetated areas. This effect causes the velocity pulses in tidal creeks. These velocity pulses are not simply caused by the sudden increase in the inundated area at the moment of flooding of the surrounding marsh platform, as explained in existing literature [e.g., *Allen*, 2000; *Pethick*, 1980]. Owing to the frictional difference between the unvegetated creeks and vegetated marsh platform, the flood wave propagates much faster through the creeks than over the platform. As a consequence, once the water level exceeds the creek banks, the flood wave propagates starting from the creeks over the platform (Figure 8e). Indeed, at this moment of flooding of the platform, the amount of water that needs to be discharged through the creek is suddenly increased, which causes the velocity pulses in the creek (Figure 3). However, if all vegetation is removed from the platform, the flood wave propagates as easy over the platform as through the creeks, so that the platform is not flooded from the creeks but by sheet flow coming from the marsh edge (Figure 8f). Consequently, if all vegetation is removed, there are no velocity pulses in the creeks (Figure 3).

[44] As the marsh platform is flooded starting from the creeks, the flow velocities are rapidly reduced on the platform owing to friction caused by the vegetation cover. As a result, sedimentation rates are highest just next to the creeks and decrease with increasing distance from the creeks as a consequence of progressive sediment trapping (Figure 8). In contrast, in between vegetated areas, flow velocities are enhanced, which results in reduced sediment deposition (Figure 8).

[45] In the vertical dimension, the transition from emergent to submerged vegetation leads to changes in the spatial flow pattern. During conditions with emergent vegetation (i.e., beginning and end of an inundation cycle), flow directions are perpendicular to the creeks (Figure 5f). During conditions with submerged vegetation, the difference in flow resistance between the unvegetated creeks and vegetated platform reduces, so that large-scale sheet flow develops over the marsh platform, starting from and perpendicular to the seaward open boundary and crossing vegetated and unvegetated areas (Figure 5h). As a result, sedimentation patterns will be spatially more homogeneous once the vegetation is overtopped (Figure 11). This vegetation effect explains the changing flow directions during inundation of a marsh platform, as reported from field studies [*Christiansen et al.*, 2000; *Davidson-Arnott et al.*, 2002; *Leonard*, 1997; *Wang et al.*, 1993].

[46] Although the model has not yet been applied for a long timescale but only for a single inundation event, the model simulations so far suggest that the presence of a vegetation cover is responsible for two geomorphic features that are typical for tidal marshes: (1) the formation and maintenance of tidal creeks, and (2) the formation of levees just next to tidal creeks. First, the model simulations showed that at the marsh edge, where the vegetation starts to colonize the unvegetated mudflat in typical patches, flow velocities are enhanced in between the vegetation patches, leading to reduced sediment deposition (Figure 8). If erosion would be considered in the model (which, for simplicity, was not the case in this study), the enhanced flow velocities in between vegetated patches may have caused erosion in between these vegetation patches. The question may be raised whether in the long-term this
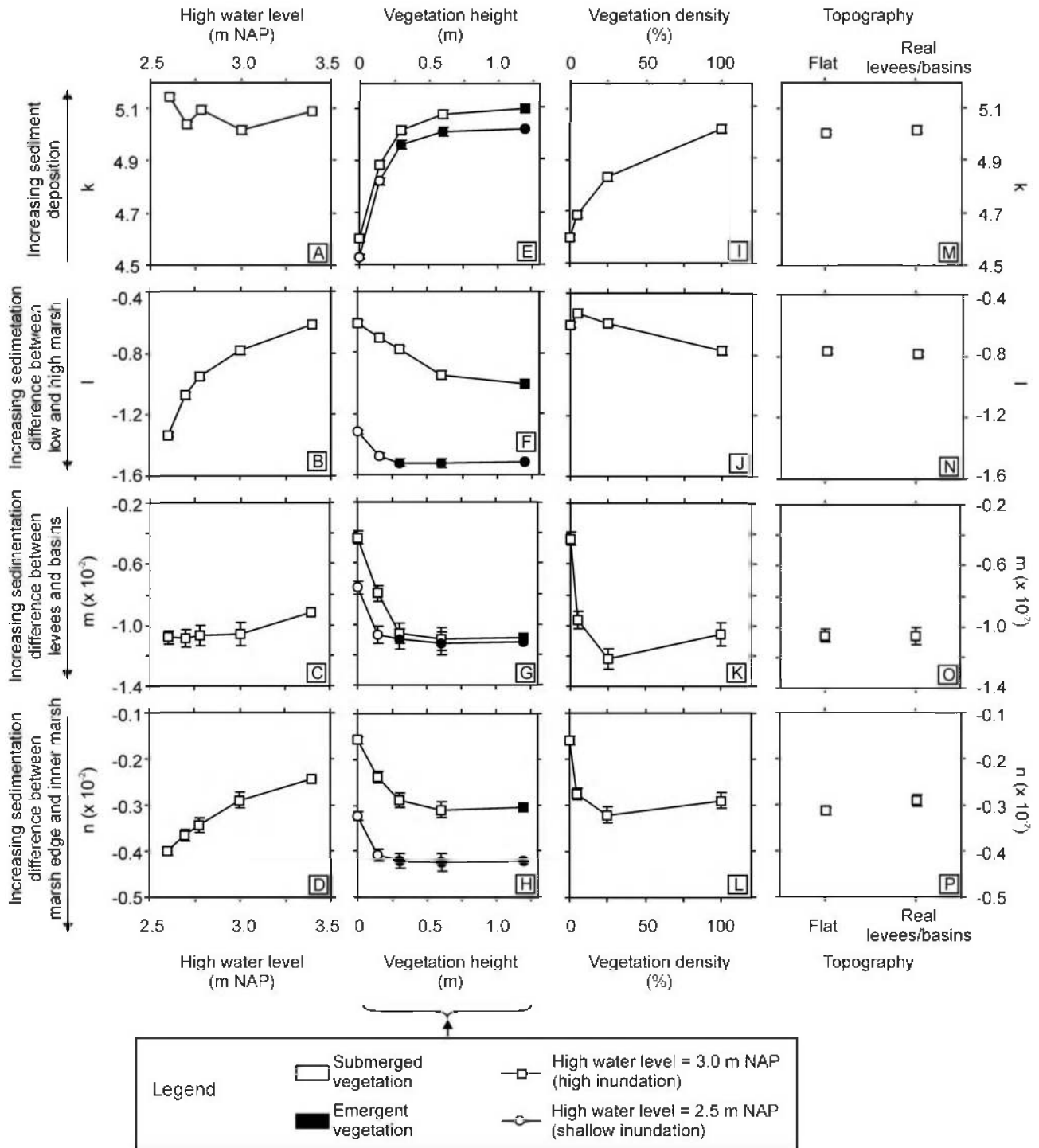
Figure 11. Influence of different model variables on the simulated spatial sedimentation pattern: (a–d) k, l, m, and n (i.e., regression parameters in equation (11)) versus high water level (for constant vegetation height 0.3 m, density 100%, real levee-basin topography); (e–h) k, l, m, and n versus vegetation height (for two high water levels (see legend), vegetation density 100%, real levee-basin topography); (i–l) k, l, m, and n versus vegetation density (for constant high water level 3 m NAP, vegetation height 0.3 m, real levee-basin topography), (M-P) micro-topography of the high marsh platform (for constant high water level 3 m NAP, vegetation height 0.3 m, vegetation density 100%). Here 100% vegetation density is density as observed in the field. Each circle in these graphs represents data for one simulated inundation cycle. Error bars represent 95% confidence intervals for the regression parameter estimates. For all regression analyses, $R^2 > 0.85$.

mechanism would lead to the formation of tidal creeks. In order to simulate long-term tidal creek formation and evolution, erosion should be included in the model [e.g., *Fagherazzi and Furbish*, 2001; *Fagherazzi and Sun*, 2004]. Although creeks are also observed on unvegetated tidal mudflats, the simulations further suggest that the geometry of tidal marsh creeks is affected by the presence of vegetation. If no vegetation were present, no velocity pulses would occur in the tidal marsh creeks (Figure 3), leading to sediment infilling of the creeks (Figures 8g and 8h). In the long term, this would mean that tidal creeks would be less deep and possibly less wide if no vegetation would be present. Second, the model results suggest that, without vegetation cover, flow perpendicular to the creeks would be negligible (Figures 8f and 9), so that the decrease in sedimentation rates with increasing distance from the creeks would not be as rapid as with vegetation (Figures 8g, 8h and 11e−11l). In the long term, this would mean that the formation of levees and basins, as observed in tidal marshes, would not be so pronounced if no vegetation would be present. Indeed, levees are generally not developed along tidal creeks that are present on unvegetated mudflats. Similar effects of vegetation cover on levee formation may be expected on river floodplains.

[47] Although our short-term, single-tide simulations clearly show the crucial impact of vegetation on flow and sedimentation patterns, we must be careful when extrapolating our short-term results to implications for the long-term development of tidal marsh landforms. Up to now, our model results suggest that the presence of a vegetation cover leads to the long-term development of tidal channels, levees and basins. In the long term, feedback mechanisms may occur, which reduce the vegetation effect on landform. For example, as levees become higher than basins, the levees will be less flooded so that sediment deposition on the levees decreases, until the elevation difference between levees and basins has reached an equilibrium [*Temmerman et al.*, 2004a]. Furthermore, in the long term, we may expect feedback mechanisms between geomorphic changes and changes in vegetation patterns. For example, vegetated areas may expand laterally over neighboring unvegetated areas, until flow velocities in between vegetated areas are so enhanced that erosion occurs and prevents further expansion of the vegetation. Up to now, however, it remains unsolved to what extent such feedback mechanisms between vegetation, flow and geomorphology result in the long-term in self-organized spatial patterns of both vegetation and geomorphology. With this study, we demonstrated that interactions between vegetation, flow and sediment transport are crucial to understand single-tide flow and sedimentation patterns in a tidal marsh landscape.

References

Allen, J. R. L. (1994), A continuity-based sedimentological model for temperate-zone tidal salt marshes, *J. Geol. Soc., 151*, 41–49.

Allen, J. R. L. (2000), Morphodynamics of Holocene salt marshes: A review sketch from the Atlantic and southern North Sea coasts of Europe, *Quat. Sci. Rev., 19*(12), 1155–1231.

Baptist, M. J. (2003), A flume experiment on sediment transport with flexible, submerged vegetation, paper presented at International Workshop on Riparian Forest Vegetated Channels: Hydraulic, Morphological and Ecological Aspects, RIPFOR, Trento, Italy.

Bates, P. D., M. G. Anderson, D. A. Price, R. J. Hardy, and C. N. Smith (1996), Analysis and development of hydraulic models for floodplain flows, in *Floodplain Processes*, edited by M. G. Anderson, D. E. Walling, and P. D. Bates, pp. 215–254, John Wiley, Hoboken, N. J.

Bayliss-Smith, T. P., R. Healey, R. Lailey, T. Spencer, and D. R. Stoddart (1979), Tidal flow in salt marsh creeks, *Estuarine Coastal Shelf Sci., 9*, 235–255.

Beffa, C., and R. J. Connell (2001), Two-dimensional flood plain flow: Part I. Model description, *J. Hydraul. Eng., 6*, 397–405.

Bouma, T. J., M. B. De Vries, E. Low, L. Kusters, P. M. J. Herman, I. C. Tanczos, A. Hesselink, S. Temmerman, P. Meire, and S. Van Regenmortel (2005a), Hydrodynamic measurements on a mudflat and in salt marsh vegetation: Identifying general relationships for habitat characterisations, *Hydrobiologia, 540*, 259–274.

Bouma, T. J., M. B. De Vries, E. Low, G. Peralta, I. Tanczos, J. Van de Koppel, and P. M. J. Herman (2005b), Trade-offs related to ecosystem-engineering: A case study on stiffness of emerging macrophytes, *Ecology, 86*, 2187–2199.

Chen, M. S., S. Wartel, and S. Temmerman (2005), Seasonal variation of flocculation on tidal flats, the Scheldt estuary, *Hydrobiologia, 540*, 181–195.

Christiansen, T., P. L. Wiberg, and T. G. Milligan (2000), Flow and sediment transport on a tidal salt marsh surface, *Estuarine Coastal Shelf Sci., 50*, 315–331.

Davidson-Arnott, R. G. D., D. Van Proosdij, J. Ollerhead, and L. Schostak (2002), Hydrodynamics and sedimentation in salt marshes: Examples from a macrotidal marsh, Bay of Fundy, *Geomorphology, 48*(1–3), 209–231.

Fagherazzi, S., and D. J. Furbish (2001), On the shape and widening of salt marsh creeks, *J. Geophys. Res., 106*, 991–1003.

Fagherazzi, S., and T. Sun (2004), A stochastic model for the formation of channel networks in tidal marshes, *Geophys. Res. Lett., 31*, L21503, doi:10.1029/2004GL020965.

Fischer-Antze, T., T. Stoesser, P. Bates, and N. R. B. Olsen (2001), 3D numerical modelling of open-channel flow with submerged vegetation, *J. Hydraul. Res., 39*(3), 303–310.

French, J. R., and T. Spencer (1993), Dynamics of sedimentation in a tide-dominated backbarrier salt marsh, Norfolk, U.K., *Mar. Geol., 110*(3-4), 315–331.

French, J. R., and D. R. Stoddart (1992), Hydrodynamics of salt marsh creek systems: Implications for marsh morphological development and material exchange, *Earth Surf. Processes Landforms, 17*, 235–252.

Hibma, A., H. J. De Vriend, and M. J. F. Stive (2003), Numerical modelling of shoal pattern formation in well-mixed elongated estuaries, *Estuarine Coastal Shelf Sci., 57*, 981–991.

Horritt, M. S. (2000), Calibration of a two-dimensional finite element flood-flow model using satellite radar imagery, *Water Resour. Res., 36*(11), 3279–3291.

Koppejan, H. (2000), Toelichting bij de vegetatiekartering Westerschelde 1998, report, Rijkswaterstaat, Meetkundige Dienst, Delft, Netherlands.

Lane, S. N. (1998), Hydraulic modelling in hydrology and geomorphology: A review of high resolution approaches, *Hydrol. Proc., 12*, 1131–1150.

Lawrence, D. S. L., J. R. L. Allen, and G. M. Havelock (2004), Salt marsh morphodynamics: An investigation of tidal flows and marsh channel equilibrium, *J. Coastal Res., 20*, 301–316.

Leonard, L. A. (1997), Controls on sediment transport and deposition in an incised mainland marsh basin, southeastern North Carolina, *Wetlands, 17*(2), 263–274.

Leonard, L. A., and M. E. Luther (1995), Flow hydrodynamics in tidal marsh canopies, *Limnol. Oceanogr., 40*(8), 1474–1484.

Lesser, G., J. Roelvink, J. Van Kester, and G. Stelling (2004), Development and validation of a three-dimensional morphological model, *Coastal Eng., 51*, 883–915.

Lopez, F., and M. H. Garcia (2001), Mean flow and turbulence structure of open-channel flow through non-emergent vegetation, *J. Hydraul. Eng., 127*, 392–402.

Marani, M., E. Belluco, A. D'Alpaos, A. Defina, S. Lanzoni, and A. Rinaldo (2003), On the drainage density of tidal networks, *Water Resour. Res., 39*(2), 1040, doi:10.1029/2001WR001051.

Mudd, S. M., S. Fagherazzi, J. T. Morris, and D. J. Furbish (2004), Flow, sedimentation, and biomass production on a vegetated salt marsh in South Carolina: Toward a predictive model of marsh morphologic and ecologic evolution, in *The Ecogeomorphology of Tidal Marshes, Coastal*

Estuarine Stud., vol. 59, edited by S. Fagherazzi, M. Marani, and L. K. Blum, pp. 165–188, AGU, Washington, D. C.

Nash, J. E., and J. V. Sutcliffe (1970), River flow forecasting through conceptual models: Part I. A discussion of principles, *J. Hydrol., 10,* 282–290.

Neary, V. S. (2003), Numerical solution of fully developed flow with vegetative resistance, *J. Eng. Mech., 129*(5), 558–563.

Nepf, H. M. (1999), Drag, turbulence, and diffusion in flow through emergent vegetation, *Water Resour. Res., 35*(2), 479–489.

Nepf, H. M., and E. R. Vivoni (2000), Flow structure in depth-limited, vegetated flow, *J. Geophys. Res., 105,* 547–557.

Nicholas, A. P., and C. A. Mitchell (2003), Numerical simulation of overbank processes in topographically complex floodplain environments, *Hydrol. Proc., 17,* 727–746.

Nichols, W. F., K. T. Killingbeck, and P. V. August (1998), The influence of geomorphological heterogeneity on biodiversity: II. A landscape perspective, *Conserv. Biol., 12*(2), 370–379.

Partheniades, E. (1965), Erosion and deposition of cohesive soils, *J. Hydraul. Div. Am. Soc. Civ. Eng., 91,* 105–131.

Pethick, J. S. (1980), Velocity surges and asymmetry in tidal channels, *Estuarine Coastal Shelf Sci., 11,* 331–345.

Philips, N. A. (1957), A co-ordinate system having some special advantages for numerical forecasting, *J. Meteorol., 14,* 184–185.

Reed, D. J., D. R. Stoddart, and T. P. Bayliss-Smith (1985), Tidal flows and sediment budgets for a salt-marsh system, Essex, England, *Vegetatio, 62,* 375–380.

Rinaldo, A., S. Fagherazzi, S. Lanzoni, M. Marani, and E. Dietrich (1999), Tidal networks: 3. Landscape-forming discharges and studies in empirical geomorphic relationships, *Water Resour. Res., 35*(12), 3919–3929.

Rodi, W. (1980), *Turbulence Models and Their Applications in Hydraulics: A State of the Art Review*, Int. Assoc. for Hydraul. Res., Delft, Netherlands.

Shi, Z., J. S. Pethick, and K. Pye (1995), Flow structure in and above the various heights of a saltmarsh canopy: A laboratory flume study, *J. Coastal Res., 11,* 1204–1209.

Temmerman, S., G. Govers, S. Wartel, and P. Meire (2003), Spatial and temporal factors controlling short-term sedimentation in a salt and fresh-water tidal marsh, Scheldt estuary, Belgium, SW Netherlands, *Earth Surf. Processes Landforms, 28,* 739–755.

Temmerman, S., G. Govers, P. Meire, and S. Wartel (2004a), Simulating the long-term development of levee-basin topography on tidal marshes, *Geomorphology, 63*(1-2), 39–55.

Temmerman, S., G. Govers, S. Wartel, and P. Meire (2004b), Modelling estuarine variations in tidal marsh sedimentation: Response to changing sea level and suspended sediment concentrations, *Mar. Geol., 212,* 1–19.

Temmerman, S., T. J. Bouma, G. Govers, and D. Lauwaet (2005), Flow paths of water and sediment in a tidal marsh: Relations with marsh developmental stage and tidal inundation height, *Estuaries, 28*(3), 338–352.

Uittenbogaard, R. E. (2003), Modelling turbulence in vegetated aquatic flows, paper presented at International Workshop on Riparian Forest Vegetated Channels: Hydraulic, Morphological and Ecological Aspects, RIPFOR, Trento, Italy.

Wang, F. C., T. S. Lu, and W. B. Sikora (1993), Intertidal marsh suspended sediment transport processes, Terrebonne Bay, Louisiana, U.S.A, *J. Coastal Res., 9,* 209–220.

WL|Delft Hydraulics (2003), *User Manual Delft3D-FLOW*, Delft, Netherlands.

Woolnough, S. J., J. R. L. Allen, and W. L. Wood (1995), An exploratory numerical model of sediment deposition over tidal marshes, *Estuarine Coastal Shelf Sci., 41,* 515–543.

T. J. Bouma and P. M. J. Herman, Netherlands Institute of Ecology (NIOO-KNAW), Centre for Estuarine and Marine Ecology, Korringaweg 7, NL-4401 NT Yerseke, Netherlands.

M. B. De Vries and Z. B. Wang, WL|Delft Hydraulics, Rotterdamseweg 185, NL-2629 HD Delft, Netherlands.

G. Govers, Katholieke Universiteit Leuven, Physical and Regional Geography Research Group, Redingenstraat 16, B-3000 Leuven, Belgium.

S. Temmerman, Department of Biology, University of Antwerpen, Groenenborgerlaan 171, B-2020 Antwerpen, Belgium. (stijn.temmerman@ua.ac.be)